


 Cite this: *Chem. Commun.*, 2020, 56, 15643

 Received 9th October 2020,
Accepted 21st November 2020

DOI: 10.1039/d0cc06760a

rsc.li/chemcomm

Gas phase identification of the elusive oxaziridine (cyclo-H₂CONH) – an optically active molecule†

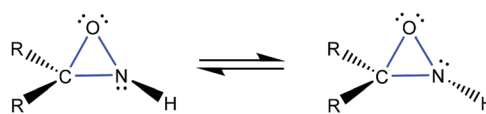
 Santosh K. Singh,^{ab} Jesse La Jeunesse,^{ab} Cheng Zhu,^{ab} N. Fabian Kleimeier,^{ab} Kuo-Hsin Chen,^c Bing-Jian Sun,^c Agnes H. H. Chang^{*c} and Ralf I. Kaiser^{ib}*^{ab}

The hitherto elusive oxaziridine molecule (cyclo-H₂CONH) – an optically active, high energy isomer of nitrosomethane (CH₃NO) – is prepared in processed methane–nitrogen monoxide ices and detected upon sublimation in the gas phase. Electronic structure calculations reveal likely routes *via* addition of carbene (CH₂) to the nitrogen–oxygen double bond of nitrosyl hydride (HNO). Our findings provide a fundamental framework to explore the preparation and stability of racemic oxaziridines exploited in chiral substrate-controlled diastereoselective preparation such as Sharpless asymmetric epoxidation, thus advancing our fundamental understanding of the preparation and chemical bonding of strained rings in small organic molecules.

For more than half a century, oxaziridines – organic molecules featuring a strained three-membered heterocycle ring containing carbon together with two electronegative atoms (oxygen, nitrogen) (Scheme 1) – have attracted considerable interest from the theoretical chemistry, physical organic, and synthetic organic communities from a fundamental point of view of diverse chemical bonding and electronic structure due to their chirality^{1–5} and exceptional high barriers of ring inversion processes⁶ of the nitrogen atom allowing for the possibility of chirality at the nitrogen center.⁶ First reported by Emmons *et al.*,⁷ oxaziridine derivatives have emerged as key reagents in organic chemistry^{8–11} for an array of oxidations involving Sharpless asymmetric epoxidations^{11,12} and aziridination of olefins¹³ along with α -hydroxylation of enolates¹⁴ often involving chiral substrate-controlled diastereoselective preparations. Whereas nitrogen and oxygen classically act as nucleophiles due to their high electronegativities of 3.04 and 3.44 on the Pauling scale, oxaziridines promote an electrophilic transfer of both heteroatoms, in which the outcome of the chemical reaction is driven by the electrophilic

character of each atom. These reactions involve oxygen transfer *via* cycloaddition reactions, which often involve exotic diradical characters of the transition state to reaction.^{8,11} This unconventional reactivity is based on the highly strained three-membered ring with a relatively weak N–O bond elongated to 151 to 152 pm¹⁵ compared to traditional nitrogen–oxygen single bonds of 106 to 140 pm. Although oxaziridines do not incorporate an asymmetric carbon atom and hence fail Pasteur's traditional definition of chirality,¹⁶ oxaziridines signify a benchmark of chiral ring compounds, in which the nitrogen inversion barrier of up to 133 kJ mol^{–1} can be associated with an augmented repulsion of the non-bonding electron pairs of the adjacent oxygen and nitrogen atoms.^{6,17,18} Oxaziridines also act as intermediates to amides and take part in [3+2] cycloadditions with heterocumulenes to synthesize substituted five-membered heterocycles.¹² The potential role of oxaziridine in transition metal complexes like cobalt salicylaldehyde (Co[salicylaldehyde]₂) highlights the significance in preparative, synthetic chemistry.¹⁹

However, regardless of the importance of oxaziridines, the oxaziridine molecule (cyclo-H₂CONH; **1**) itself has not been isolated to date considering hitherto overwhelming experimental difficulties in preparing suitable precursor molecules eventually forming molecule **1** (Fig. 1 and Table S1, ESI†). As a structural isomer of nitrosomethane (CH₃NO; **3**), formamide (NH₂CHO; **6**),²⁰ formaldehyde oxime (H₂CNOH; **4**),²¹ the 1,3-dipolar *N*-oxide methanimine (H₂CNHO; **2**),²² methanimidic acid (HNCHOH; **5**),²³ and (methyleneoxonio)amide (H₂CONH; **7**), the elusive **1** is linked *via* a substantial ring-opening barrier of 231 kJ mol^{–1} to the thermodynamically favorable isomer **2**.²⁴ This barrier competes favorably with a nearly isoenergetic transition



Scheme 1 The three membered ring structure of oxaziridine molecule exhibiting inversion at the nitrogen center. 'R' represents an (in)organic group.

^a Department of Chemistry, University of Hawaii, 2545 McCarthy Mall, Honolulu, HI 96822, USA. E-mail: ralfk@hawaii.edu

^b W. M. Keck Research Laboratory in Astrochemistry, University of Hawaii, Honolulu, HI 96822, USA

^c Department of Chemistry, National Dong Hwa University, Shoufeng, Hualien 974, Taiwan. E-mail: hhchang@gms.ndhu.edu.tw

† Electronic supplementary information (ESI) available. See DOI: 10.1039/d0cc06760a

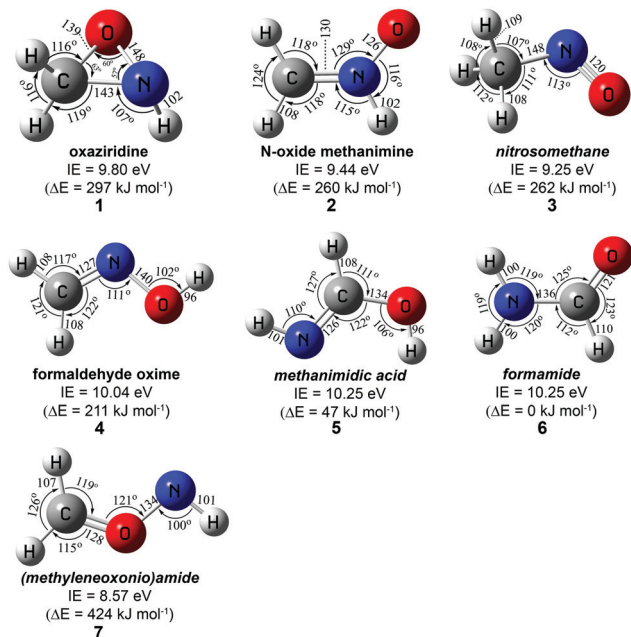


Fig. 1 Adiabatic ionization energies (IE) and relative energies (ΔE) are calculated at the CCSD/cc-pVTZ//CCSD(T)/CBS level of theory. The Cartesian coordinates of the structures are provided in Table S8 (ESI[†]). Bond lengths and angles are given in picometers and degrees, respectively.

state connecting isomers 2 with 3 through a hydrogen atom shift from the nitrogen to the carbon atom.²⁵ These energetics highlight the need for an unconventional preparative route to the elusive molecule 1.

In this study, we convey the first preparation and detection of the hitherto elusive oxaziridine molecule in the gas phase. Merging our experiments with electronic structure calculations, we reveal that compound 1 can be synthesized in low temperature ices ultimately *via* cycloaddition of carbene (CH_2) to the nitrogen–oxygen double bond of nitrosyl hydride (H-N=O). Experiments were carried out in an ultrahigh vacuum (UHV) surface science machine at a base pressure of a few 10^{-11} torr (Fig. S1, ESI[†]).²⁶ Binary ices of methane (CH_4), D4-methane (CD_4) or ^{13}C -methane ($^{13}\text{CH}_4$) with nitrogen monoxide (NO) were prepared in separate experiments with thicknesses of $743 \pm 50 \text{ nm}$ at $4.8 \pm 0.1 \text{ K}$ at ratios of $1.1 \pm 0.4 : 1$ (Fig. S2–S5 and Tables S3–S5, ESI[†]). Bond-cleavage processes in (isotopically labeled) methane and nitrogen monoxide were triggered by subjecting these ices to energetic electrons at doses of $0.44 \pm 0.04 \text{ eV molecule}^{-1}$ for methane and $0.82 \pm 0.08 \text{ eV molecule}^{-1}$ for nitrogen monoxide on average (Table S6, ESI[†]). Fourier transform infrared (FTIR) spectra of the ices were collected *in situ* before and after the irradiation (Fig. S2–S4, ESI[†]). The low irradiation dose along with overlapping infrared absorptions of functional groups of nitrogen–oxygen carrying (in)organic species does not allow an explicit identification of molecule 1 *via* FTIR spectroscopy, and hence a novel approach is clearly essential. The molecular species formed in the irradiated ices along with the reactants were sublimed by increasing the temperature of the target at a rate of 1 K min^{-1} to 320 K (temperature programmed desorption; TPD). The subliming neutral molecules were ionized exploiting tunable vacuum

ultraviolet (VUV) photoionization (PI); the ions formed were mass resolved in a reflectron time-of-flight mass spectrometer (PI-ReTOF-MS). By systematically tuning the photon energies to 10.49 eV, 9.95 eV, 9.92 eV, 9.50 eV, and 9.00 eV (Table S7, ESI[†]), the isomers 1 to 7 can be (selectively) ionized based on their adiabatic ionization energies (IE; Tables S1 and S10, ESI[†]) to elucidate which isomer(s) is(are) prepared. It shall be stressed that an evaluation of three experimentally available benchmarks – formamide, formaldehyde oxime, and nitrosomethane – with ionization energies computed at the CCSD/cc-pVTZ//CCSD(T)/CBS level of theory reveals that the calculated ionization energies can be lower by 0.02 eV or higher by 0.04 eV (Table S1, ESI[†]). This agrees with the error range determined for the calculated ionization energies of multiple molecular systems (Table S2, ESI[†]). Further, detailed calibration experiments exposed that the electric field of the extraction plate of the ion optics of the Re-TOF-MS lowers the ionization energies by 0.03 eV.²⁷

The mass spectra of the species subliming from the irradiated methane–nitrogen monoxide ices are depicted in Fig. 2 as a function of temperature recorded at photon energies of 10.49 eV, and 9.50 eV. The mass spectra measured at photon energies of 9.95 eV and 9.92 eV are shown in Fig. S6 (ESI[†]). Analyzing the experiment at 10.49 eV, a comparison of the data of the non-irradiated ice mixture (blank; Fig. S7, ESI[†]) with the exposed ices uncovers the formation of new molecules. Besides the reactant nitrogen monoxide (NO) ($m/z = 30$; IE = 9.26 eV) and prominent signal at $m/z = 46$ (NO_2), 60 (N_2O_2), 75 ($\text{C}_2\text{H}_5\text{NO}_2$), and 90 ($\text{C}_2\text{H}_6\text{N}_2\text{O}_2$), the PI-ReTOF-MS data of the CH_4 –NO system reveal a noticeable trace at mass-to-charge (m/z) of $m/z = 45$ (Fig. 3A); at 10.49 eV, this TPD graph shows three sublimation events peaking at 100 K, 165 K, and 265 K. The mass-to-charge ratio of $m/z = 45$ can be associated with the molecular formula CH_3NO . It is important to highlight that at a photon energy of 10.49 eV, all isomers 1 to 7 can be photoionized; signal at $m/z = 45$ does not exist in the control experiment (Fig. S7, ESI[†]) revealing that ion counts at $m/z = 45$ are linked to the radiation exposure of the binary ice mixture. To provide evidence that the molecule monitored *via* $m/z = 45$ is connected to a species with the formula CH_3NO , isotopic experiments were conducted by replacing methane (CH_4) in separate experiments with ^{13}C -methane ($^{13}\text{CH}_4$) and D4-methane (CD_4).

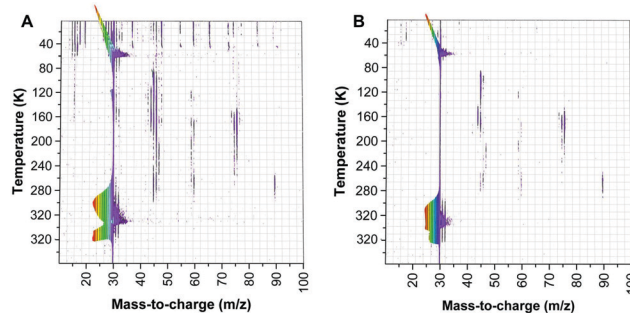


Fig. 2 PI-ReTOF mass spectra measured at photoionization energies of (A) 10.49 eV and (B) 9.50 eV during the temperature program desorption (TPD) phase of the irradiated methane (CH_4) – nitrogen monoxide (NO) ices.

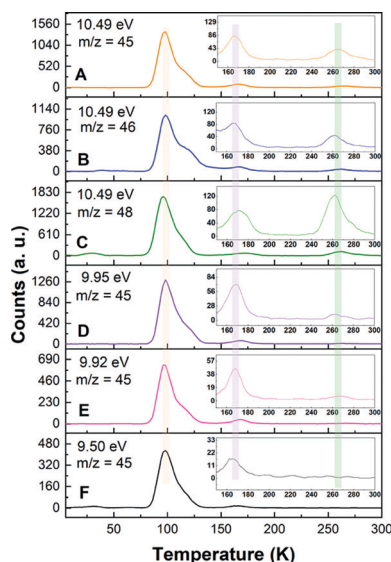


Fig. 3 Temperature program desorption (TPD) profiles measured at (A) $m/z = 45$ ($\text{CH}_4 + \text{NO}$), (B) $m/z = 46$ ($^{13}\text{CH}_4 + \text{NO}$), and (C) $m/z = 48$ ($\text{CD}_4 + \text{NO}$) using a photon energy of 10.49 eV. TPD profiles of $m/z = 45$ ($\text{CH}_4 + \text{NO}$) at photoionization energies of (D) 9.95 eV, (E) 9.92 eV and (F) 9.50 eV. Errors in the photon energies are ± 0.0001 eV.

The TPD profiles recorded at $m/z = 46$ and 48 are shifted by 1 amu and 3 amu in the ^{13}C - and D-labeled ices, respectively (Fig. 3B and C). These findings suggest that for the sublimation events peaking 100 K, 165 K, and 265 K, the molecule of interest contains one oxygen atom along with a single carbon atom and three hydrogen atoms – a conclusion which is coherent with the molecular formula CH_3NO .

Having provided compelling evidence on the formation of molecule(s) with the molecular formula CH_3NO (45 amu) along with its ^{13}C - and D-substituted counterparts, we extract now the nature of the structure isomer. This goal is accomplished by selectively photoionizing discrete isomers based on their distinct ionization energies (Fig. 1 and Table S1, ESI[†]). Lowering the photon energy to 9.95 eV and 9.92 eV still photoionizes isomers 1, 2, 3 and 7. However, these energies are below the adiabatic ionization energies of isomers 4 to 6. A detailed inspection of Fig. 3A–E reveals that all three sublimation events at 100 K, 165 K, and 265 K are still present albeit with lower ion counts due to the reduced photoionization cross section at lower photon energies. Once the photon energy is lowered to 9.50 eV, isomers 2 and 3 – if formed – can still be ionized, but this energy is below the adiabatic ionization energy of isomer 1. At 9.50 eV, ion counts are clearly visible for the sublimation events at 100 K and 165 K; these events can be correlated with the formation of isomer(s) 3 and/or 2. However, the sublimation event at 265 K disappears at 9.50 eV revealing that these ion counts are connected to the formation of the previously elusive isomer 1. The TPD profiles recorded for $m/z = 45$ at 10.49 eV, 9.95 eV, and 9.92 eV reveal identical pattern after scaling (Fig. S8, ESI[†]). At 9.0 eV, the sublimation events at 100 K and 165 K disappear as well (Fig. S9, ESI[†]). This implies that these peaks centred at 100 and 165 K cannot be assigned to isomer 7, but to isomers 2 and/or 3; therefore isomer 7 is not formed in our

experiments. Comparison of sublimation profile of nitrosomethane measured previously in nitromethane (CH_3NO_2) matrix²⁸ with the TPD profile obtained in the present study at $m/z = 45$, suggests that sublimation event centred at 100 K can be attributed to isomer 3 (Fig. S10, ESI[†]). Therefore, based on the photoionization studies along with isotope substitution experiments within the methane–nitrogen monoxide system, oxaziridine parent molecule is clearly prepared and detected. It should be noted here that since we have used energetic electrons, no enantiomeric excess is expected as evidenced from our previous studies on the formation of amino acids.^{29,30}

Having elucidated the preparation of isomer 1, we are exploring now possible mechanism(s) of its formation (Fig. 4). Experiments of pure methane ices at low doses and temperatures revealed three decomposition pathways leading to methyl (CH_3) (reaction (1)) and singlet/triplet carbene (CH_2) (reactions (2a/2b)). The methyl radical and the hydrogen atom may react with nitrogen monoxide barrierlessly if both reagents have a favorable recombination geometry in the ices to form isomer 3 (reaction (3)) and nitrosyl hydride (HNO) (reaction (4)) in exoergic reactions, respectively. The reactivity of carbene (CH_2) with nitrosyl hydride (HNO) strongly depends on the spin state of carbene.

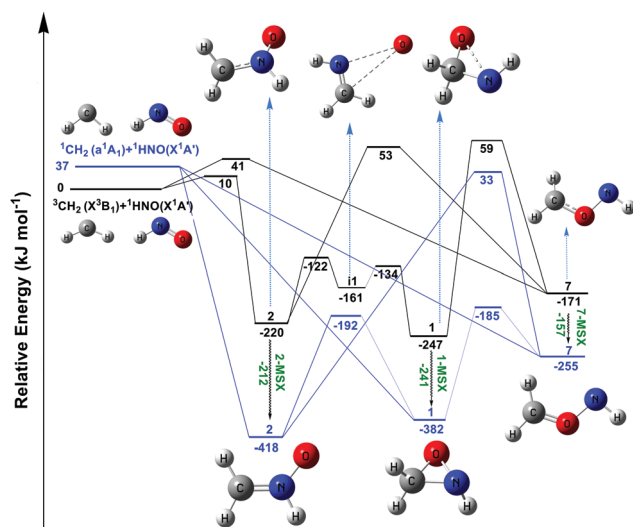
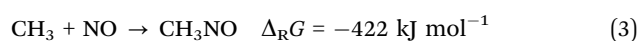
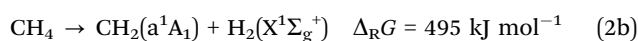


Fig. 4 Computationally predicted reaction pathways of singlet (blue) and triplet (black) carbene (CH_2) with nitrosyl hydride (HNO). The CCSD/cc-pVTZ//CCSD(T)/CBS energies are given in kJ mol^{-1} with respect to the separated reactants. The CPMSCF/TZVPP//CCSD(T)/CBS minimum-energy crossing points (MSX) are shown for inter system crossing (ISC) pathways as waved arrows. Geometrical parameters of the species depicted are provided in Fig. S12–S14 (ESI[†]) and coordinates are tabulated in Table S9 (ESI[†]). Bond lengths and angles are given in picometers and degrees, respectively.

The electronic structure calculations at the CCSD/cc-pVTZ//CCSD(T)/CBS level of theory revealed that singlet carbene may add barrierlessly to the nitrogen atom, the oxygen atom, and to the nitrogen–oxygen double bond of nitrosyl hydride (HNO) forming isomers **2**, **7**, and **1**, respectively (Fig. 4 and Tables S9, S11, ESI†). These barrierless entrance channels are supported by the intrinsic reaction coordinate (IRC) calculations performed at the CCSD/cc-pVTZ//CCSD(T)/CBS level of theory (Fig. S11, ESI†). These products (**2**, **1**, and **7**) are stabilized by 418, 382, and 255 kJ mol⁻¹ with respect to the separated reactants. Both the intermediates **2** and **7** can undergo ring closure to form **1** after crossing energy barriers of 226 and 70 kJ mol⁻¹, respectively. However, isomerization of intermediate **7** to isomer **1** is more facile due to smaller energy barrier therefore, we could not observe **7** in our experiments. On the triplet potential energy surface, addition of triplet carbene to the central nitrogen and to the terminal oxygen atom of nitrosyl hydride (HNO), leading to triplet **2** and **7**, have entrance barriers of 10 and 41 kJ mol⁻¹, respectively. In spite of several attempts, we could not locate the reaction path leading from the reactants to triplet **1**; therefore, it appears that **1** cannot originate from the reaction of triplet reactants in one step. However, triplet **1** might be produced from triplet **2** via two-step pathway: (i) elimination of oxygen atom from **2** leading to a van der Waals complex **i1** followed by (ii) recombination of oxygen atom to methylene group. Both the steps have well-defined transition states which are higher in energy by about 98 and 86 kJ mol⁻¹ with respect to the triplet **2**. Triplet **7** could also isomerize to **1** in a single-step after crossing an energy barrier of 230 kJ mol⁻¹. The triplet species (**2**, **1**, and **7**) could undergo intersystem crossing (ISC) to the singlet manifold via minimal energy crossing points (MSX) which are depicted in Fig. S12 (ESI†). It is important to note here that the N–O bond length in triplet **1** is larger (227 pm) than the conventional covalent bond and thus triplet **1** does not represent a true cyclic structure (Fig. S13, ESI†). Overall, the computations suggest that the barrierless addition of singlet carbene to the nitrogen–oxygen double bond of nitrosyl hydride (HNO) is a feasible pathway to form molecule **1**. It is important to highlight that the addition of singlet carbene to a double bond of nitrosyl hydride (HNO) mimic the reactivity of carbene with ethylene (C₂H₄) leading to the formation of cyclopropane (C₃H₆) in electron irradiated methane–ethylene ices at 5 K.³¹

In conclusion, this study reveals the preparation and detection of the chiral oxaziridine (**1**) – a high energy isomer of nitrosomethane (**3**). The molecule **1** originates in the methane–nitrogen monoxide ice mixture after exposure to energetic electrons and was detected by exploiting a tunable single photon vacuum ultraviolet (VUV) photoionization coupled with reflectron time-of-flight mass spectrometry (PI-ReTOF-MS). Non-equilibrium reaction pathways leading to **1** were proposed; barrierless addition of the singlet carbene with nitrogen–oxygen double bond of nitrosyl hydride (HNO) appeared to be the most likely pathway for the formation of aforementioned molecule. The molecule **1** reveals elongated nitrogen–oxygen (148 pm), carbon–nitrogen (143 pm), and carbon–oxygen (139 pm) bonds in contrast to the carbon–carbon bond (151 pm) in cyclopropane.³² A high ring inversion barrier of 143 kJ mol⁻¹

(Fig. S15 and Tables S12, S13, ESI†) – allows the possibility of chirality in oxaziridine – an exotic isomer of nitrosomethane previously undetected.

The experimental work was supported by the US Army Research Office (W911NF1810438). KHC, BJS, and AHHC thank the National Center for High-performance Computer in Taiwan for providing the computer resources in the calculations.

Conflicts of interest

There are no conflicts to declare.

Notes and references

- 1 L. L. Lewis, L. L. Turner, E. A. Salter and D. H. Magers, *THEOCHEM*, 2002, **592**, 161–171.
- 2 M. T. Taghizadeh, M. Vatanparasad and S. Nasirianfar, *Chem. J. Mold.*, 2015, **10**, 77–88.
- 3 R. D. Bach and O. Dmitrenko, *J. Am. Chem. Soc.*, 2006, **128**, 4598–4611.
- 4 M. Polášek, M. Sadílek and F. Tureček, *Int. J. Mass Spectrom.*, 2000, **195–196**, 101–114.
- 5 S. K. Singh, T.-Y. Tsai, B.-J. Sun, A. H. H. Chang, A. M. Mebel and R. I. Kaiser, *J. Phys. Chem. Lett.*, 2020, **11**, 5383–5389.
- 6 I. Rajyaguru and H. S. Rzepa, *J. Chem. Soc., Perkin Trans. 2*, 1987, 359–363.
- 7 W. D. Emmons, *J. Am. Chem. Soc.*, 1957, **79**, 5739–5754.
- 8 K. S. Williamson, D. J. Michaelis and T. P. Yoon, *Chem. Rev.*, 2014, **114**, 8016–8036.
- 9 G. D. Sala and A. Lattanzi, *ACS Catal.*, 2014, **4**, 1234–1245.
- 10 J. Aubé, *Chem. Soc. Rev.*, 1997, **26**, 269–277.
- 11 K. N. Houk, J. Liu, N. C. DeMello and K. R. Condroski, *J. Am. Chem. Soc.*, 1997, **119**, 10147–10152.
- 12 F. A. Davis and A. C. Sheppard, *Tetrahedron*, 1989, **45**, 5703–5742.
- 13 Q.-Q. Cheng, Z. Zhou, H. Jiang, J. H. Siitonen, D. H. Ess, X. Zhang and L. Kürti, *Nat. Catal.*, 2020, **3**, 386–392.
- 14 F. A. Davis and B. C. Chen, *Chem. Rev.*, 1992, **92**, 919–934.
- 15 M. Michalski, A. J. Gordon and S. Berski, *Struct. Chem.*, 2019, **30**, 2181–2189.
- 16 J. Gal, *Chirality*, 2011, **23**, 1–16.
- 17 A. Rauk, *J. Am. Chem. Soc.*, 1981, **103**, 1023–1030.
- 18 M. Alcamí, J. L. G. D. Paz and M. Yáñez, *J. Comput. Chem.*, 1989, **10**, 468–478.
- 19 L. Martiny and K. A. Jørgensen, *J. Chem. Soc., Perkin Trans. 1*, 1995, 699–704.
- 20 J. F. Arenas, J. C. Otero, D. Peláez and J. Soto, *J. Org. Chem.*, 2006, **71**, 983–991.
- 21 D. C. Frost, W. M. Lau, C. A. McDowell and N. P. C. Westwood, *J. Phys. Chem.*, 1982, **86**, 3577–3581.
- 22 M. Polášek and F. Tureček, *J. Am. Chem. Soc.*, 2000, **122**, 525–531.
- 23 V. V. Turovtsev, I. V. Stepanov, A. N. Kizin and Y. D. Orlov, *Russ. J. Phys. Chem. A*, 2007, **81**, 317–319.
- 24 L. Yang, X. Li, Y. Zeng, S. Zheng, L. Meng and Y. Zhao, *Acta Chim. Sin.*, 2011, **69**, 577–584.
- 25 A. E. DePrince III and D. A. Mazziotti, *J. Chem. Phys.*, 2010, **133**, 034112.
- 26 B. M. Jones and R. I. Kaiser, *J. Phys. Chem. Lett.*, 2013, **4**, 1965–1971.
- 27 A. Bergantini, M. J. Abplanalp, P. Pokhilko, A. I. Krylov, C. N. Shingledecker, E. Herbst and R. I. Kaiser, *Astrophys. J.*, 2018, **860**, 108.
- 28 P. Maksyutenko, M. Förstel, P. Crandall, B.-J. Sun, M.-H. Wu, A. H. H. Chang and R. I. Kaiser, *Chem. Phys. Lett.*, 2016, **658**, 20–29.
- 29 M. Förstel, P. Maksyutenko, B. M. Jones, B. J. Sun, H. C. Lee, A. H. H. Chang and R. I. Kaiser, *Astrophys. J.*, 2016, **820**, 117.
- 30 P. D. Holtom, C. J. Bennett, Y. Osamura, N. J. Mason and R. I. Kaiser, *Astrophys. J.*, 2005, **626**, 940–952.
- 31 M. J. Abplanalp, S. Góbi and R. I. Kaiser, *Phys. Chem. Chem. Phys.*, 2019, **21**, 5378–5393.
- 32 H. A. Skinner, *Nature*, 1947, **160**, 902.